3

Beam Steerable and Circular Polarization Reconfigurable Antenna

This chapter presents a beam steerable and circular polarization reconfigurable antenna with the ability to steer its radiation beam in different directions along with switchable circular polarization. The antenna consists of two E-shaped driven patches, a tunable phase shifter integrated with PIN diodes for pattern switching, and four switchable feeding probes for implementing polarization agility. The proposed antenna can simultaneously switch its polarization and beam. Beam switching and polarization agility are independently controlled by altering the OFF-ON states of diodes loaded on the feed network and switchable feeding probes. For the validity of the proposed concept, the antenna prototype is fabricated and tested. The proposed antenna has measured impedance bandwidth (S_{11} < -10 dB) and 3 dB axial ratio bandwidths of 23% and 17.4%, respectively, for all states over the frequency range 4.7-5.6 GHz. The measured and simulation results show that the antenna can scan up to ±30° with five reconfigurable beams and two polarization states for each reconfigurable beam.

3.1 Introduction

Circularly polarized antennas are preferable over linearly polarized antennas due to their flexibility in the orientation alignment between transmitting and receiving antennas and minimizing the fading losses caused by the multipath effect. Several methods to realize circular polarization (CP) have been studied. In general, the polarization reconfigurable antenna can be realized using two methods. In the first method, polarization is achieved by introducing some disrupting segments in the antenna's radiating structure as in [128]-[132]. While in the second method, a switchable feed network is used [76]-[133]. In [128], CP is achieved by truncating the opposite corners, while in [59], a slit is inserted in the circular microstrip antenna. However, these techniques suffer from very narrow bandwidth, which limits their practical applications. To overcome this problem, several impedance broadening techniques have been investigated using the U slot [60]-[129], L-probe [130], and E-shaped patches [63]-[132]. These designs provide wider impedance and axial ratio bandwidth. However, these designs can reconfigure only one characteristic of the antenna rather than multiple characteristics. Also, biasing circuit is designed on the radiating layer, which affects the antenna radiation performance.

Compared to single-parameter reconfigurable antennas, multiple-parameter reconfigurable antennas are more desirable because they provide more flexibility and diversity, which increase the capacity of many wireless communication systems. However, very few designs can perform hybrid reconfigurability with a single antenna structure. Recently, some designs have been reported to club two of the three reconfigurability parameters for a single antenna structure which are categorized under frequency and pattern reconfigurability [134]-[136], frequency and polarization reconfigurability [137]-[139], and pattern and polarization reconfigurability [140]-[145]. Out of these, pattern reconfigurability antennas designed to achieve polarization reconfigurability also are suitable for many applications including internet of things (IoT) and wireless local area

networks (WLAN). In [140], a cavity-backed microstrip antenna with three linear polarization states (0°, 45° and 90°) was proposed, and each polarization state can reconfigure its pattern from -20° to + 20° in the H plane. In [83], a 2x2 array antenna with polarization and pattern reconfigurable characteristics was proposed using spatial phase shift technique. This antenna can steer its polarization between RHCP and LHCP with a beam tilt of ±28°. In [142], a pattern reconfigurable antenna array with three beam scanning angles at 48°, 124° and 240° was realized using a dipole-loaded monopole slot backed by a metallic cavity. The aforementioned antennas provide both pattern and polarization reconfigurability but their large footprint and bulky three-dimensional structures limit their practical applications.

This chapter investigates a beam steerable and circular polarization reconfigurable E-shaped patch antenna which can provide wider S_{11} and AR bandwidth as reported in [131]. In previously reported CP reconfigurable E- shaped patch antennas [63]-[132], CP is achieved by varying the slot lengths using the PIN diodes/MEMS switches placed on the slots/radiating patch that severely affects the radiation pattern of the antenna [148]. This chapter addresses this issue by avoiding the switches on the radiation layer and designing the complete switching circuit on the feed layer. The feed layer is kept isolated from the radiation layer by placing it behind the antenna ground plane. In the proposed antenna, CP is achieved using four switchable probes and pattern reconfigurability is achieved through a tunable phase shifter designed using a reconfigurable feed network in chapter 2. The designed antenna can generate ten radiating modes, including five reconfigurable beams with two circular polarization states (RHCP and LHCP). The proposed design has various advantages: (a) simultaneously achieving the pattern and polarization agility using a compact profile, (b) wide impedance and 3 dB axial ratio bandwidth, and (c) minimizing the effect of PIN diodes and biasing circuits on the antenna radiation performance by placing all the switching components and biasing circuits behind the antenna ground plane.

3.2 Antenna Geometry and Reconfigurable Mechanism

3.2.1 Antenna Configuration

This chapter is the extension of the previous chapter. In Chapter 2, the proposed antenna had the limitation of narrow bandwidth and low gain in the common operating band for all states. A square E-shaped patch element is chosen to overcome the narrow bandwidth, and for the low gain, the proposed antenna is backed by a cylindrical cavity. Also, the proposed antenna had the single parameter reconfigurability characteristics. To further enhance the application potential of the previously designed antenna the multi reconfigurability is implemented by cascading the designed feed network with the four switchable feed probes.

Thus, this chapter significantly extends the chapter 2 to provide polarization reconfiguration and beam switching operation simultaneously. Fig. 3.1 represents the structure of the proposed CP-agile beam switching enable cavity-backed antenna, and its detailed dimensions are listed in Table 3.1.

The proposed antenna is printed on two stacked 1.6 mm thick FR4 substrates with a dielectric constant ε_r = 4.4 and a loss tangent tanδ = 0.02. The driven array element, placed on the bottom layer of substrate 1, is modified as a square E-shaped patch antenna element and optimized using ANSYS HFSS version 18.2 [125], as shown in Fig. 3.1(b). The feeding network layer is modified with four switchable probes shown in Fig. 3.1(c), two of which are used in each state. The inter-element spacing between the two elements is chosen as d_S = 0.55λ_0. The upper surface of substrate 2 consists of the ground plane, and the lower surface is arranged with the phase switchable power divider, including a DC biasing network, for the realization of the beam switching and polarization reconfiguration operation. The two substrates are separated by an air gap of H_a. The value of d_S and L_{f5} are optimized to achieve the wide beam switching with reduced side lobe level.

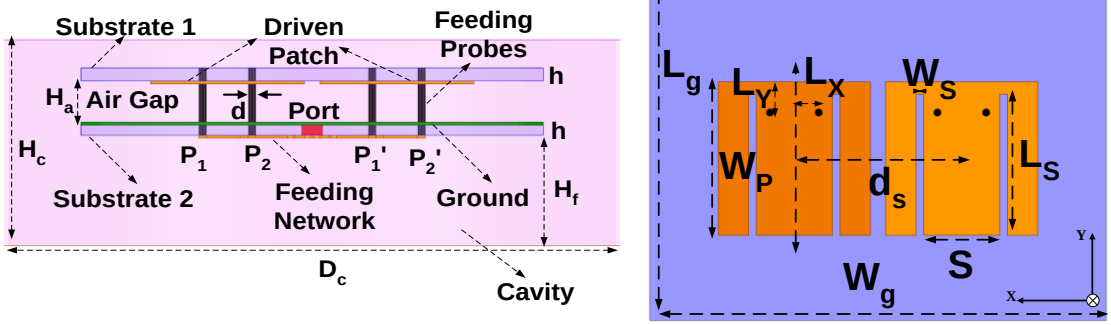

(a) (b)

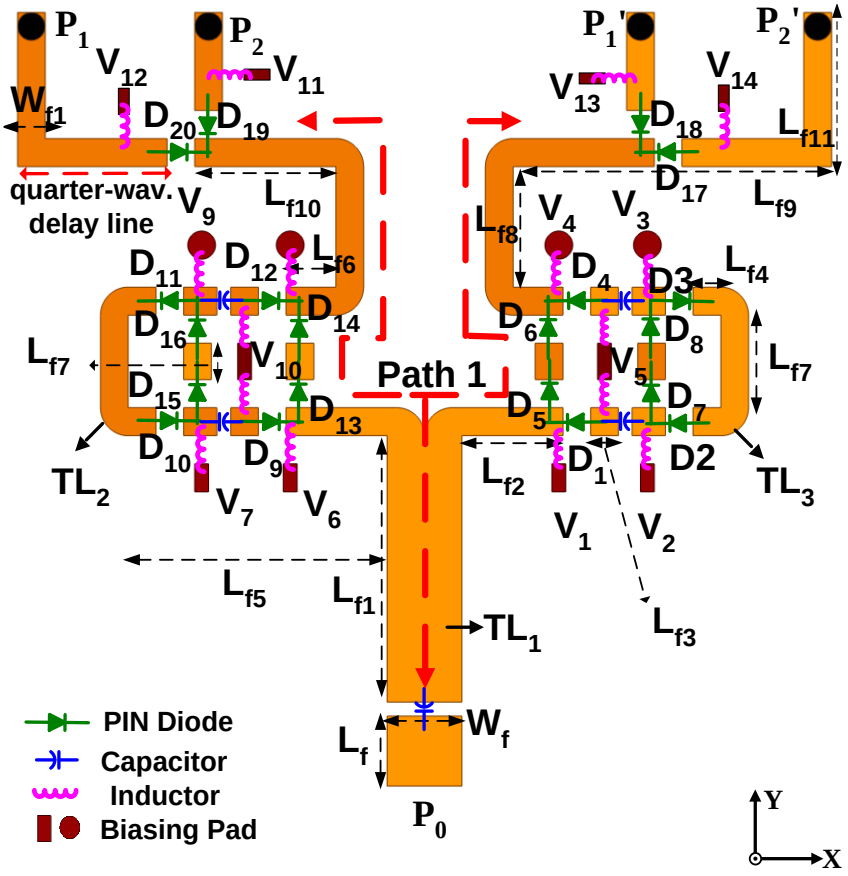

(c)

Figure 3.1: Proposed CP-agile and beam switchable array antenna structure. (a) Side view (b) Driven Patch Layer (c) Feed Network layer.

Table 3.1: **Optimized geometrical parameters of the array antenna**

Parameter	Value (mm)	Parameter	Value (mm)	Parameter	Value (mm)
L_f	2.5	L_{f8}	4.3	L_S	16.4
W_f	2.7	L_{f9}	11.5	W_S	1
W_{f1}	1	L_{f10}	5.1	H_a	6
L_{f1}	9.5	L_{f11}	5.7	H_C	35
L_{f2}	3.6	W_g	60	D_C	120
L_{f3}	1	L_g	60	d	1
L_{f4}	1	W_P	18	h	1.6
L_{f5}	9.15	S	10	H_f	23.4
L_{f6}	1.8	L_X	3.2		
L_{f7}	1.3	L_Y	4		

Table 3.2: **Biasing conditions of PIN diodes in different radiation modes**

State	Diodes condition		Beam switching	Polarization
	Forward biased	Reverse biased		
S_1	D_5, D_6, D_{13}, D_{14}, D_{18}, D_{20}	D_1-D_4, D_7-D_{12}, D_{15}, D_{16}, D_{17}, D_{19}	-18°	LHCP
S_2	D_5, D_6, D_{13}, D_{14}, D_{17}, D_{19}	D_1-D_4, D_7- D_{12}, D_{15}-D_{16}, D_{18}, D_{20}	+18°	RHCP
S_3	D_{13}, D_{14}, D_1, D_7, D_8, D_4, D_{18}, D_{20}	D_2, D_3, D_5, D_6, D_9-D_{12}, D_{15},-D_{17}, D_{19}	+26°	LHCP
S_4	D_{13}, D_{14}, D_1, D_7, D_8, D_4, D_{17}, D_{19}	D_2, D_3, D_5-D_{10}, D_{13}, D_{15}, D_{16}, D_{18}, D_{20}	+26°	RHCP
S_5	D_{13}, D_{14}, D_1, D_2, D_3, D_4, D_{18}, D_{20}	D_5-D_{12}, D_{15}-D_{17}, D_{19}	+30°	LHCP
S_6	D_{13}, D_{14}, D_1, D_2, D_3, D_4, D_{17}, D_{19}	D_5-D_{12}, D_{15}, D_{16}, D_{18}, D_{20}	+30°	RHCP
S_7	D_5, D_6, D_9, D_{15}, D_{16}, D_{12}, D_{18}, D_{20}	D_1-D_4, D_7-D_8, D_{10}-D_{11}, D_{13}-D_{14}, D_{17}, D_{19}	-26°	LHCP
S_8	D_5, D_6, D_9, D_{15}, D_{16}, D_{12}, D_{17}, D_{19}	D_1-D_4, D_7-D_8, D_{10}-D_{11}, D_{13}-D_{14}, D_{18}, D_{20}	-26°	RHCP
S_9	D_5, D_6, D_9, D_{10}, D_{11}, D_{12}, D_{18}, D_{20}	D_1-D_4, D_7-D_8, D_{13}-D_{17}, D_{19}	-30°	LHCP
S_{10}	D_5, D_6, D_9, D_{10}, D_{11}, D_{12}, D_{17}, D_{19}	D_1-D_4, D_7-D_8, D_{13}-D_{16}, D_{18}, D_{20}	-30°	RHCP

3.2.2 Beam Switching Analysis and Feed Network

To realize the reconfigurability in the radiation pattern, a phase switchable network is designed and combined with the feed line of the two-way power splitter. The zoom-in view of the reconfigurable feed network shown in Fig. 3.1(c) consists of one 50-ohm transmission line (TL_1), two 100-ohm transmission lines (TL_2 and TL_3), and twenty pin diodes. A 50-ohm excitation source excites the input port P_0 of the power splitter, and its output ports P_1, P_1', P_2, and P_2' are used to feed the driven patch element with an input impedance of 100 ohms. The different radiation beams are obtained by properly choosing the different excitation paths controlled by different PIN diodes (D_1-D_{16}). The PIN diodes BAR64-02V from Infineon Technology [124] are used as RF switches on the gaps between the adjacent transmission lines to switch among the different paths. The different modes and their corresponding diodes states and reconfigurable patterns are mentioned in Table 3.2.

3.2.3 Polarization Reconfigurability Analysis

To describe polarization agility, we have considered four different cases of the feed networks, which are referred as Ant_1 to Ant_4 as described in Fig. 3.2. Their comparative study in terms of the reflection coefficient (S_{11}) and axial ratio (AR) is shown in Fig. 3.3. In all the configurations, initially, we have fixed the transmission path 1 consisting of PIN diodes D_5, D_6, D_{13}, and D_{14} (Fig. 3.1). Ant_1 is centrally excited by feed probes P_1 and P_1' as shown in Fig. 3.2. The 10 dB impedance bandwidth of Ant_1 is observed as 28.5% (S_{11} < -10 dB from 4.8 GHz to 6.4 GHz) and an axial ratio of approximately 15 dB is observed at 4.76 GHz. To further introduce the two orthogonal components required for circular polarization, asymmetry is introduced in the structure by shifting the feed probes P_1 and P_1' by a distance Lx from their centre position, forming Ant_2. By shifting the probe, the impedance bandwidth almost remains the same, but the axial ratio of the Ant_2 is

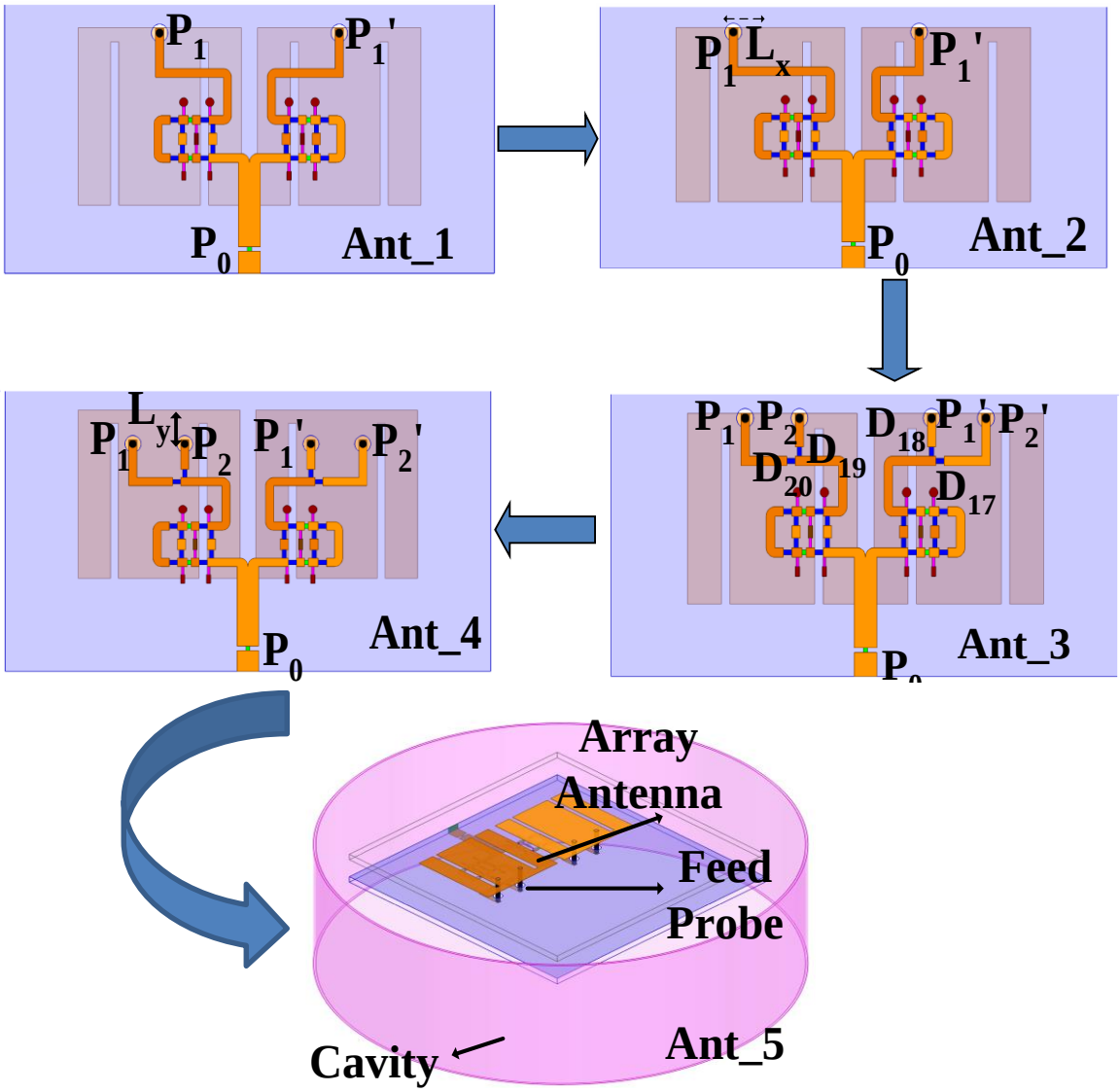

Figure 3.2: Proposed reconfigurable array antenna design evolution.

significantly increased due to the resonance frequencies of multiple modes coming together, which widens the bandwidth as discussed in [131]. For Ant_2 axial ratio remains equal to or below 3 dB in the frequency of 4.7-5.3 GHz as shown in Fig. 3.3. To introduce the polarization reconfigurability in Ant_2, two more feeding probes P_2 and P_2' are added as shown in Ant_3, which can be switched independently by using four PIN diodes (D_{17}-D_{20}). Due to the four PIN diodes and reactance produced by feeding probes, axial ratio shifted from 4.7-5.3 GHz to 4.8-5.2 GHz. In Ant_4, the four feeding probes are shifted upward by a distance Ly to again improve the AR at a higher frequency and it remains below

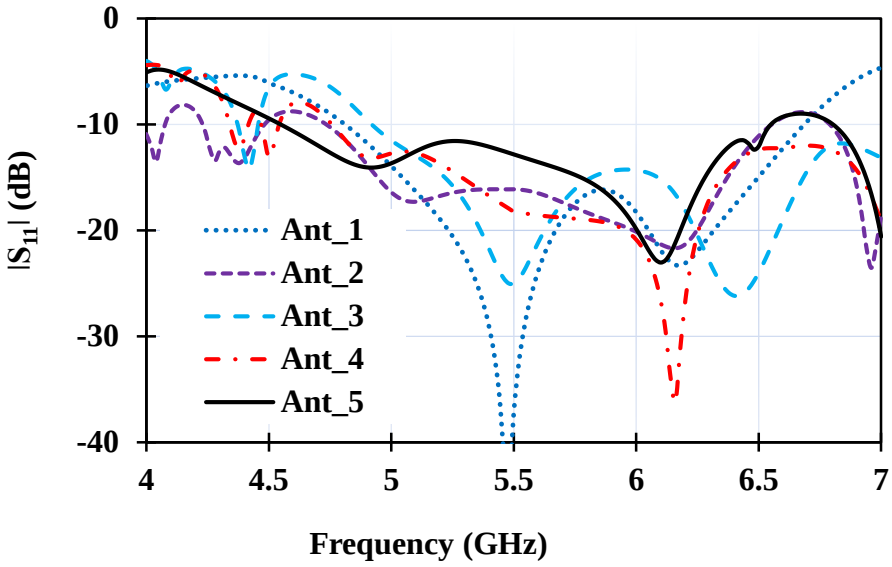

(a)

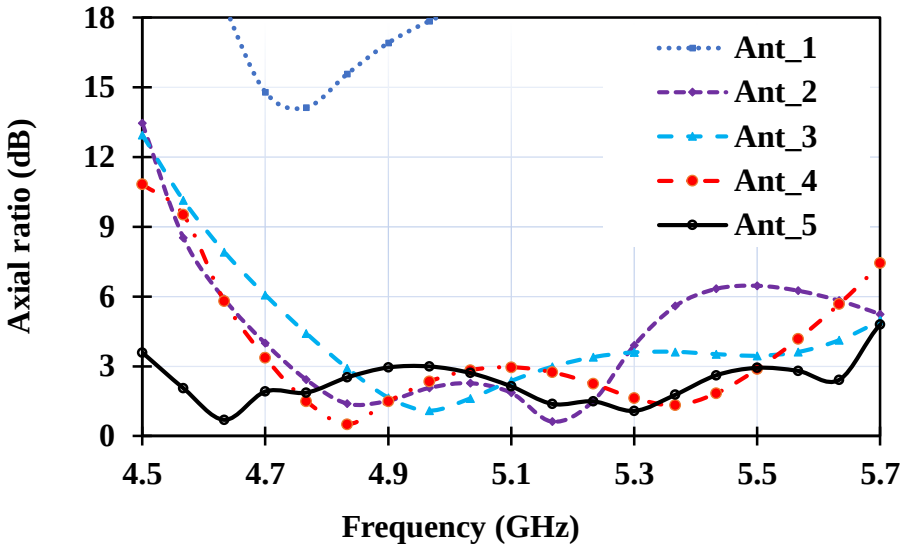

(b)

Figure 3.3: Simulated results of antenna in different cases (Ant_1-Ant_5). (a) reflection coefficient (b) axial ratio.

3 dB in the frequency of 4.7-5.5 GHz. For Ant_3 and Ant_4, the reflection coefficient and axial ratio in Fig.3.3 are shown when the antenna works in state 2 (RHCP). Furthermore, Ant_4 is modified as Ant_5 by adding a cavity that acts as a secondary radiator to generate an additional CP band to increase the axial ratio from 4.7-5.5 GHz to 4.5-5.7 GHz and improve the radiation performance as reported in [147].

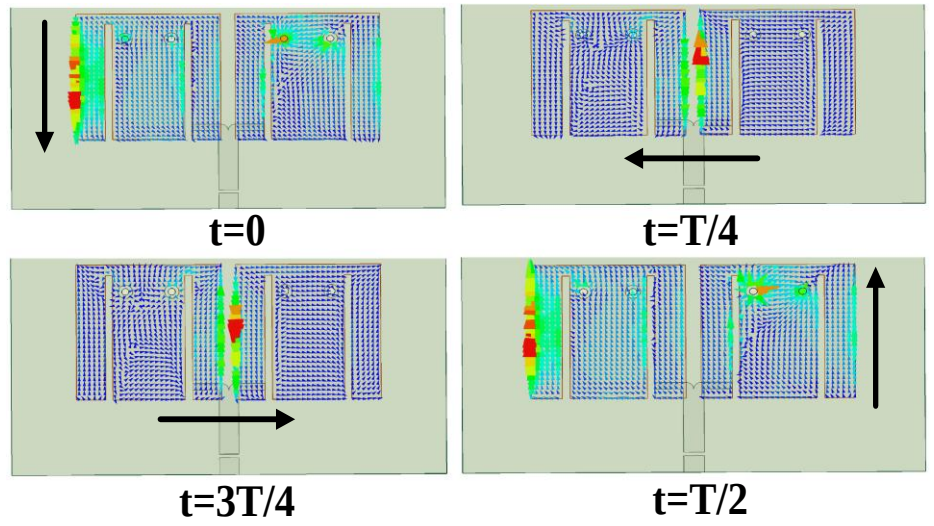

(a)

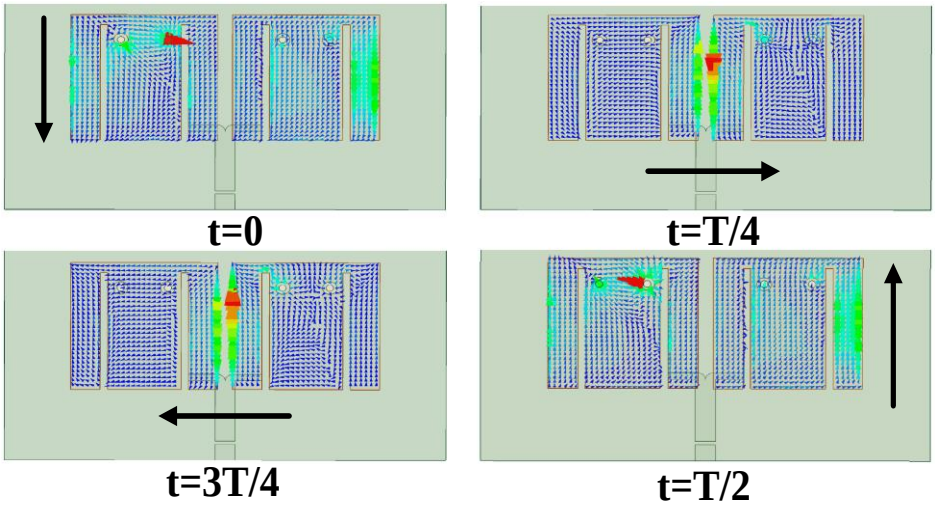

(b)

Figure 3.4: Simulated 5.2 GHz surface current distributions of the CP-agile array antenna. (a) for state 1 (LHCP) (b) for state 2 (RHCP) at four different time phases.

The surface current distributions of Ant_5 in state 1 and state 2 are shown in Fig. 3.4. In Fig. 3.4(a), the surface current vector rotates clockwise with respect to the different time phases, and it can be regarded as the two orthogonal components are in 90° phase difference that indicates the antenna works in LHCP mode. Similarly, in Fig. 3.4(b), the surface current rotates in an anticlockwise sense forming RHCP.

3.2.4 Working Principle

After designing the phase switchable feed network and four switchable feed probes, these are combined together to realize the beam switching and polarization reconfigurability independently. For S_1 and S_2 states, the two antenna elements are excited in same phase through the PIN diodes D_5, D_6, D_{13} and D_{14} (path 1) and probe P_1, P_1' and P_2, P_2' are selected for LHCP (S_1) and RHCP (S_2) operations, respectively. In S_1 state, the electrical length of L_{f9} is increased by 90° due to the quarter wavelength delay line present. As a result, there is a 90° phase difference between P_1 and P_1'. This phase difference leads to a beam shift of -18° from its broadside direction. Conversely, in S_2 state, the beam direction shifts by 18° due to the opposite phase difference. In S_3 and S_4 states, a phase difference is introduced between the elements using phase switchable network by selecting the feed path through diodes D_{13}, D_{14}, D_1, D_7, D_8, D_4 to provide the phase shift of ±26° in the radiation pattern and for LHCP probe P_1, P_1' (S_3) and for RHCP probe P_2, P_2' (S_4) are selected. Similarly, for S_5 and S_6 states, diodes D_{13}, D_{14}, D_1, D_2, D_3, D_4 are turned ON along with the probe P_1, P_1' and P_2, P_2' to provide the beam tilt of ± 30° in LHCP and RHCP modes, respectively. Same tilting beams are observed towards the –X axis due to the antenna symmetry which is represented as S_7 ~ S_{10} in Table 3.2.

Moreover, it is observed that in S_1 and S_2 states, a quarter wavelength delay line is used to control the beam direction, while in the rest of the states the combined effect of a quarter-wave delay line and the phase delay provided by the phase switchable network used to effectively control the beam direction of the system.

3.2.5 Specification of PIN Diode and its Biasing Circuit

In simulation, PIN diodes BAR64-02V from Infineon Technology are modelled using the equivalent circuit of PIN diodes for the ON and OFF states shown in Fig. 2.4 [124]. For DC bias control circuit, the value of DC blocking capacitor (C) to block the DC current and RF choke inductor (L) to block the RF current are optimized as C = 6 pF and L = 22 nH.

During measurement, an external switching circuit is designed to control the ON/OFF states of the PIN diodes. The switching circuit consists of push to ON/OFF buttons, single-pole double-throw (SPDT) switches, and LEDs (green and red) to specify negative and positive biases on the PIN diodes. Fourteen DC wires are soldered on the biasing pad (V_1-V_{14}), designed on the feed network layer. To make the structure more compact and to minimize the effect of biasing circuit on antenna radiation performance, a phase switching network and DC biasing circuit are designed on the feed network layer, as shown in Fig. 3.1(c). For achieving different pattern and polarization states, the corresponding bias voltages on the biasing pads are mentioned in Table 3.3.

Table 3.3: **Connection of dc biasing pads for different pattern and polarization states**

Bia. Voltage	**S_1**	**S_2**	**S_3**	**S_4**	**S_5**	**S_6**	**S_7**	**S_8**	**S_9**	**S_{10}**
V_1	+V	+V	-V	-V	-V	-V	+V	+V	+V	+V
V_2	OC	OC	+V	+V	-V	-V	OC	OC	OC	OC
V_3	OC	OC	-V	-V	+V	+V	OC	OC	OC	OC
V_4	-V	-V	-V	-V	-V	-V	-V	-V	-V	-V
V_5	OC	OC	+V	+V	+V	+V	OC	OC	OC	OC
V_6	+V	+V	+V	+V	+V	+V	-V	-V	-V	-V
V_7	OC	OC	OC	OC	OC	OC	+V	+V	-V	-V
V_8	-V	-V	-V	-V	-V	-V	-V	-V	-V	-V
V_9	OC	OC	OC	OC	+V	+V	-V	-V	+V	+V
V_{10}	OC	OC	OC	OC	OC	OC	+V	+V	+V	+V
V_{11}	OC	+V	OC	+V	OC	+V	OC	+V	OC	+V
V_{12}	+V	OC	+V	OC	+V	OC	+V	OC	+V	OC
V_{13}	+V	OC	+V	OC	+V	OC	+V	OC	+V	OC
V_{14}	OC	+V	OC	+V	OC	+V	OC	+V	OC	+V

3.2.6 Parametric Analysis

A parametric analysis is performed to understand further the effect of the structural parameters of the CP reconfigurable antenna on the antenna characteristics. Three important parameters, including slot length (L_s), slot width (W_s), and slot distance (S), are studied, which affect the reflection coefficient and the axial ratio of the antenna. The other parameter values as mentioned in Table 3.1, are kept constant while investigating the particular parameter. This study is performed when the antenna is working in state 1. The other states are not considered here due to brevity.

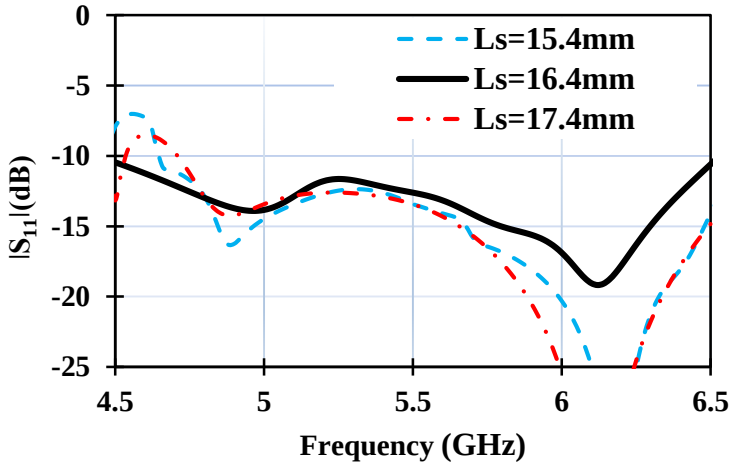

(a)

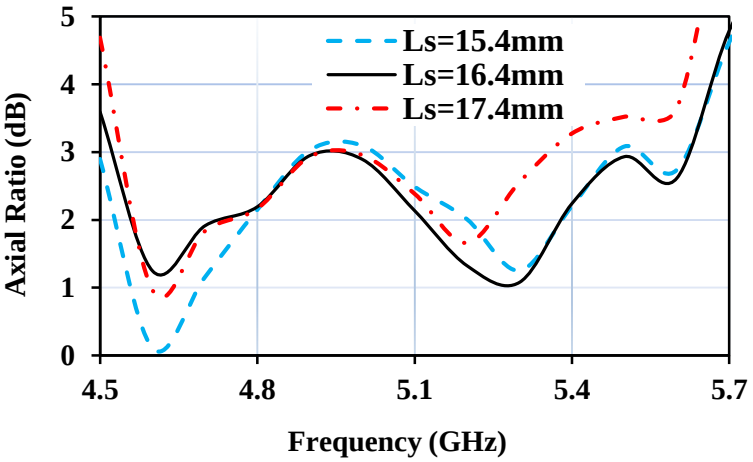

(b)

Figure 3.5: Simulated S_{11} and axial ratio characteristics of the antenna with different values of slot length (L_S). (a) S_{11} and (b) Axial Ratio.

Fig. 3.5 studies the effect of changing the slot length (L_s) on the S- parameter, and AR of the proposed antenna. As shown in Fig. 3.5(a), the impedance bandwidth almost remains the same when the slot length varies from 15.4 mm to 17.4 mm. But the AR of the antenna in Fig. 3.5(b) improves slightly near 5 GHz with the increase of L_S from 15.4 mm to 16.4mm. Further increase in the length of L_S, shifted the axial ratio above 3 dB at a higher frequency. Hence the value of *Ls* is chosen as 16.4 mm, for which the axial ratio is below 3 dB for the entire operating band.

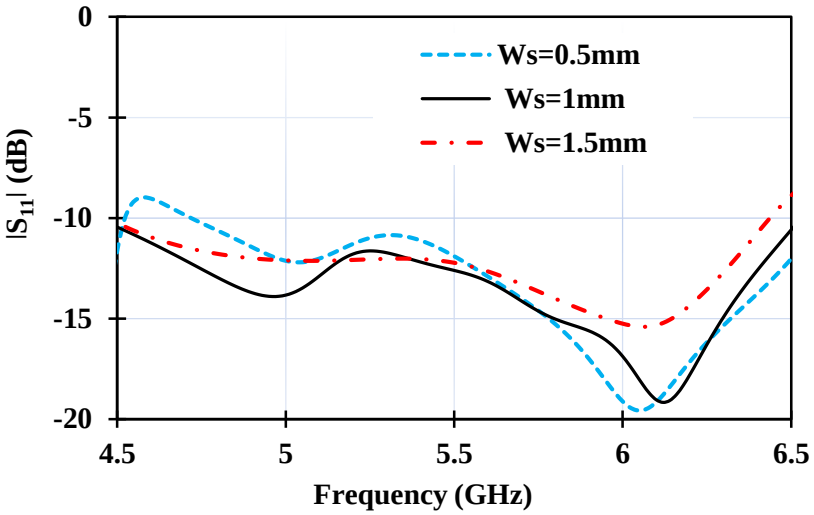

(a)

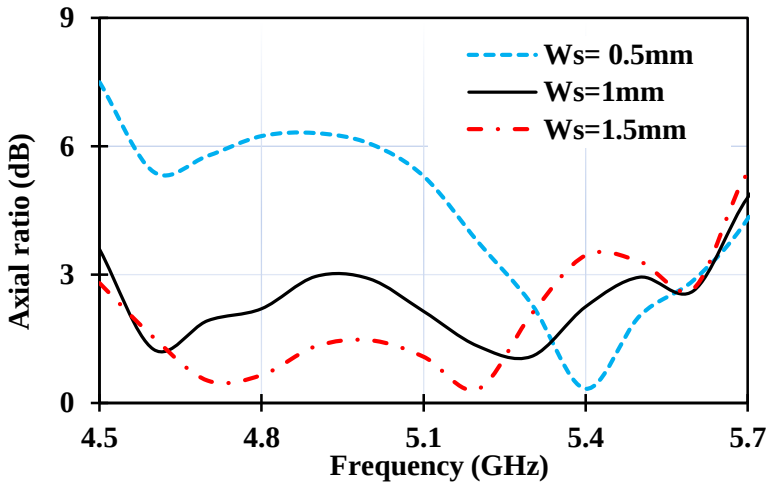

(b)

Figure 3.6: Simulated S_{11} and axial ratio characteristics of the antenna with different values of slot width (W_S). (a) S_{11} and (b) Axial Ratio.

The next parameter studied is the slot width (W_S), as shown in Fig. 3.6. It is observed that variation in slot width (W_S) has a major impact on the axial ratio but has a minor effect on the impedance matching. When the W_S is 0.5 mm, the axial ratio is above 3 dB at the lower frequency region. When W_S is increased from 0.5 mm to 1 mm, axial ratio performance improves at a lower frequency. It covers the entire operating band, and further increasing the W_S deteriorates the axial ratio beyond 5.4 GHz. Hence an intermediate value of 1 mm is chosen to cover the entire operating band.

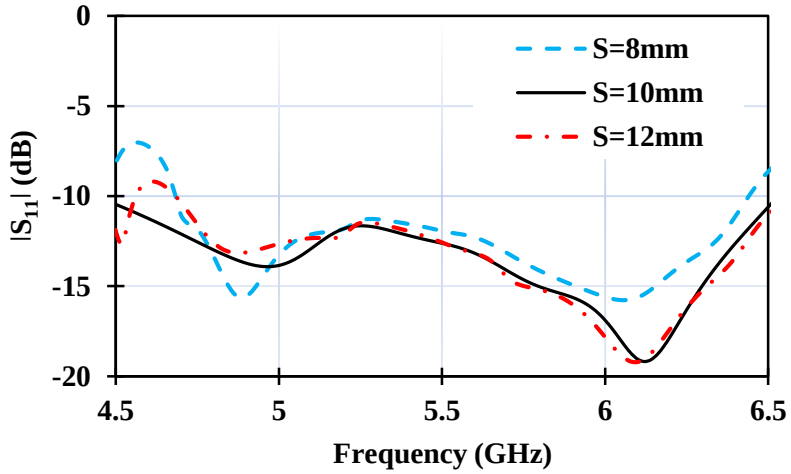

(a)

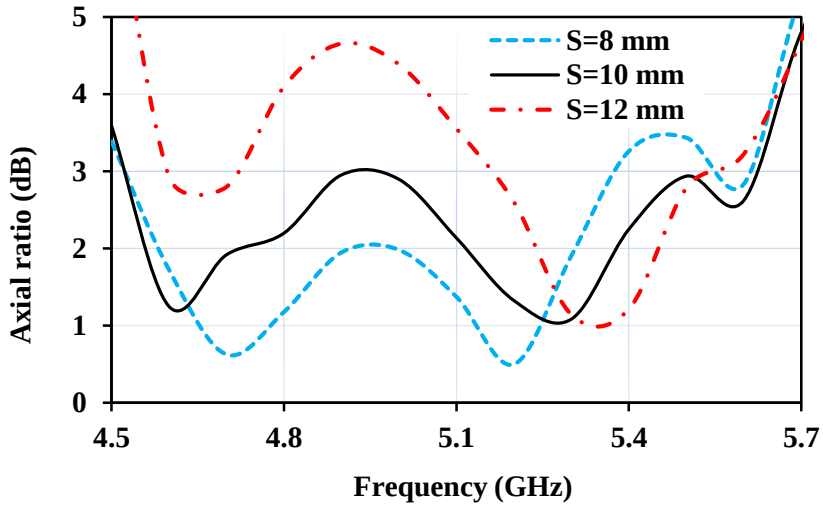

(b)

Figure 3.7: Simulated S_{11} and axial ratio characteristics of the antenna with different values of slot distance (S). (a) S_{11} and (b) Axial Ratio.

Fig. 3.7 shows the performance of the antenna when the distance between the slots (*S*) is varied from 8 mm to 12 mm, the impedance matching frequency remains the same, but the AR deteriorates around 5 GHz and the value of AR deteriorates and shifted above 3 dB.

From the parametric study, it is observed that the slot dimensions and positions are less sensitive to the reflection coefficient but have a major impact on the axial ratio performance because the phase difference between the orthogonal components reaches 90° at a certain dimension and position of the slot, and beyond this critical value the phase difference deviates from 90°.

3.3 Results and Discussion

To verify the concept, a prototype of the designed beam steerable and circular polarization reconfigurable antenna is fabricated and measured. Fig. 3.8 shows the photograph of the assembled array antenna prototype. Four nylon nuts and bolts and plastic spacers of thickness 3 mm are used at the four corners to align and support the two substrate layers.

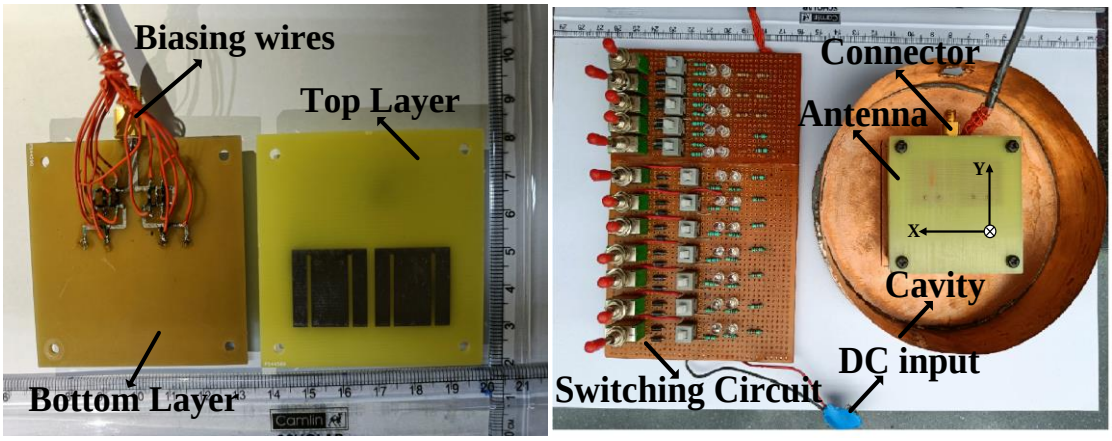

(a) (b)

Figure 3.8: Prototype of the fabricated CP agile and beam switchable array antenna. (a) feeding network layer and patch layer (b) assembled array antenna with external switching circuit.

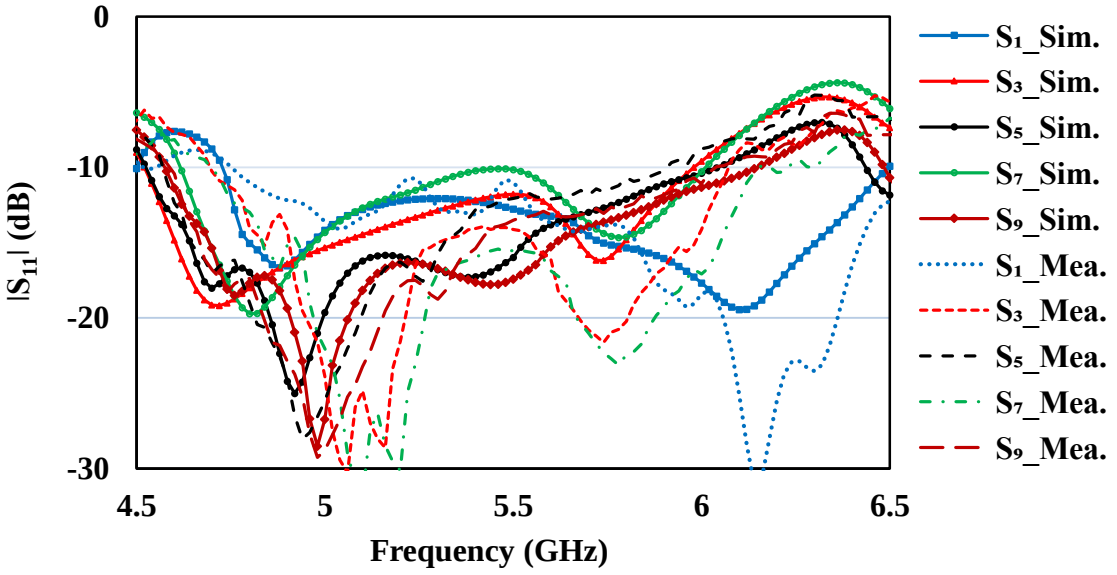

(a)

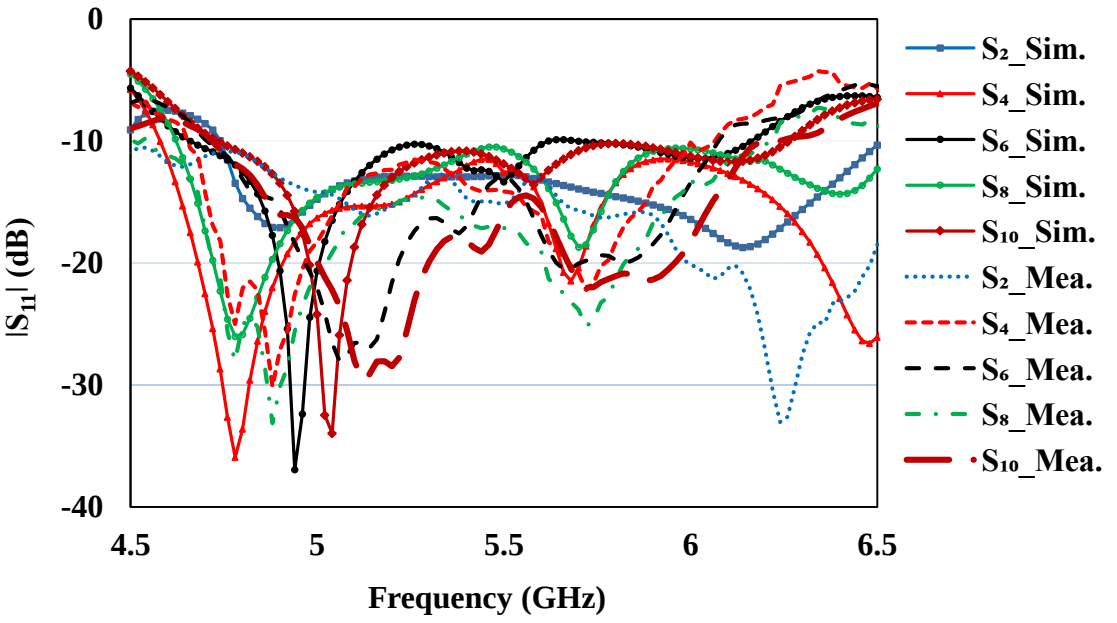

(b)

Figure 3.9: The proposed array antenna measured and simulated S-parameter in (a) LHCP mode (b) RHCP mode.

In the experiment, an external switching circuit is employed to select the feeding probes and to turn the states of the PIN diodes to control the polarization and pattern states of the antenna. The reflection coefficient of the proposed antenna array is measured under different switching states by Anritsu VNA Master MS2038C. Measured results for LHCP

and RHCP modes are plotted in Fig. 3.9, where the corresponding simulation results are also included for comparison. Some discrepancies are observed between simulated and measured results. As mentioned in [119], these discrepancies are mainly due to the approximate modeling of the PIN diodes, DC bias circuit, and soldering quality that affects the simulation accuracy. Fig. 3.9 shows the measured overlapped impedance bandwidth for S_{11} < -10 dB is approximately 26.4% for all operating polarization and radiation beam states over the frequency range 4.6 GHz to 6 GHz.

The measurement of the radiation pattern, gain, and the axial ratio is carried out in the anechoic chamber where the magnitude and phase of E_θ and E_ϕ far-field components of the radiated electric field are measured to calculate the axial ratio. Further axial ratio is calculated using the equations:

$$E_{RHCP} = \frac{1}{\sqrt{2}} (E_\theta + j\, E_\Phi) \quad (3.1)$$

$$E_{LHCP} = \frac{1}{\sqrt{2}} (E_\theta - j\, E_\Phi) \quad (3.2)$$

$$\text{AR} = \frac{(|E_{RHCP}| + |E_{LHCP}|)}{(|E_{RHCP}| - |E_{LHCP}|)} \quad (3.3)$$

Fig.3.10, compares the measured and corresponding simulated results of axial ratio properties in the direction of maximum radiation in LHCP and RHCP modes for different radiation beams. A good agreement is observed between the simulated and measured results. The measured 3 dB axial ratio bandwidth can cover a frequency band from 4.7 GHz to 5.6 GHz. The simulated and measured gain for different states are compared in Fig. 3.11. The measured gain ranges from 6.7 dBi to 8.5 dBi for LHCP mode and 6.5 dBi to 8.8 dBi for RHCP mode. So the proposed beam steerable and circular polarization reconfigurable antenna have overlapped bandwidth of 23% for both S_{11} < -10 dB and 3 dB AR over the frequency range 4.7 GHz to 5.6 GHz.

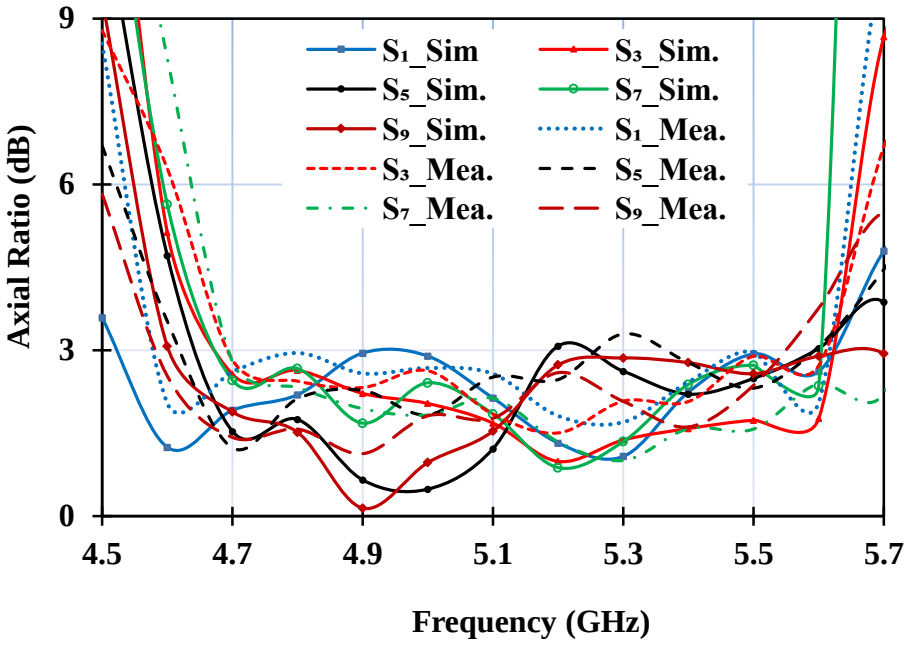

(a)

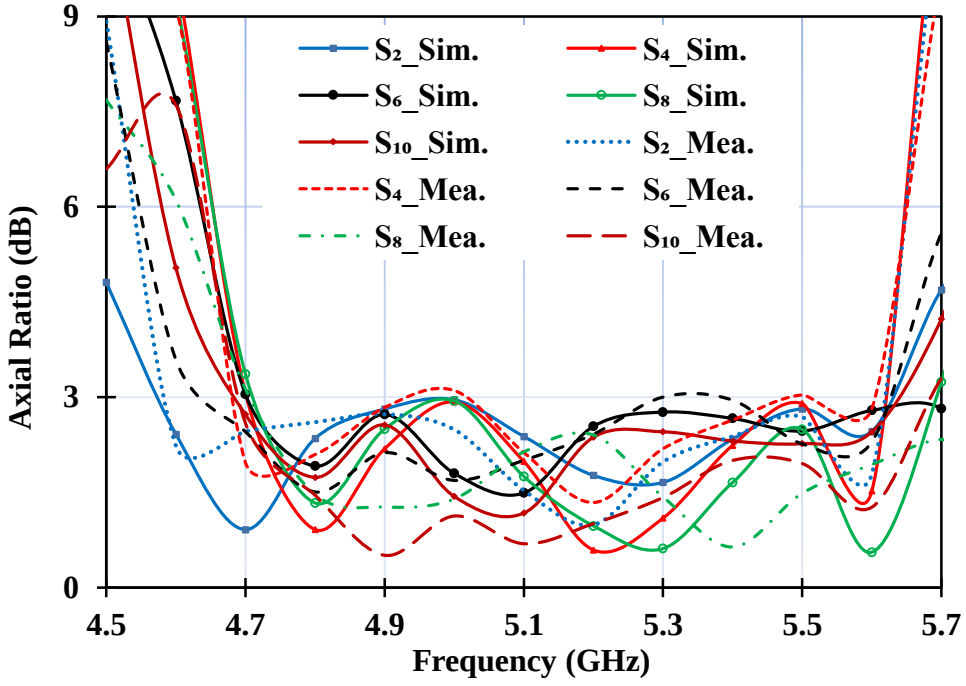

(b)

Figure 3.10: The proposed array antenna measured and simulated axial ratios in (a) LHCP mode (b) RHCP mode.

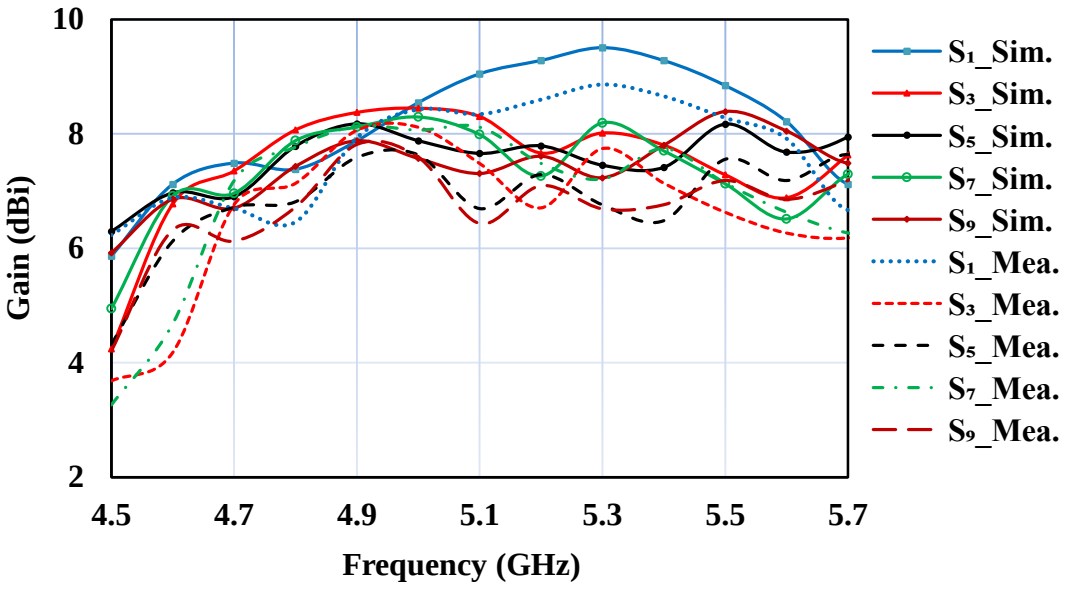

(a)

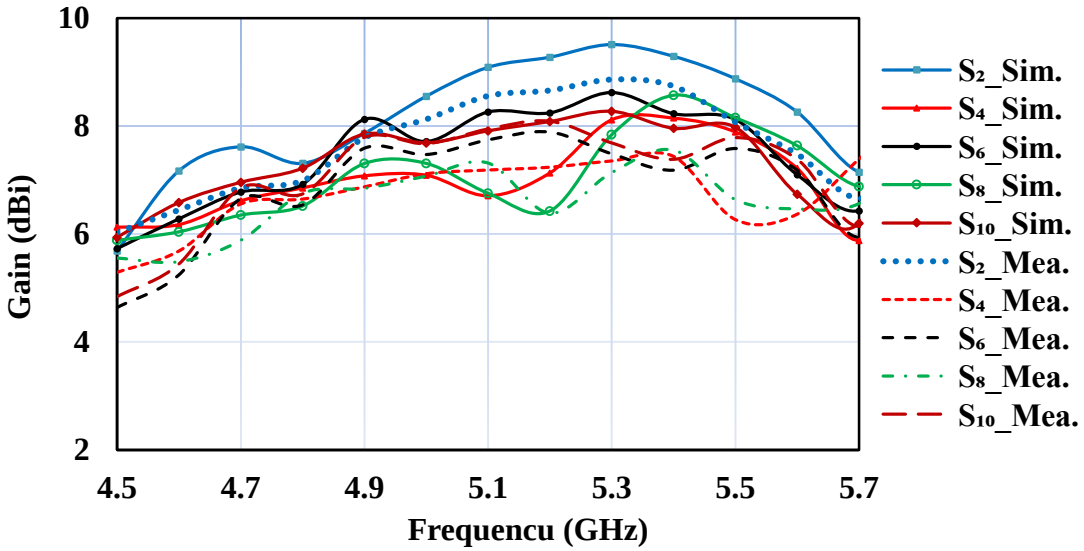

(b)

Figure 3.11: The proposed array antenna measured and simulated peak gain in (a) LHCP mode (b) RHCP mode.

The normalized measured and simulated radiation patterns at the XZ cut plane are compared at the center frequency for different operating states (S_1-S_{10}), as shown in Fig. 3.12. During pattern measurements, the DC wires, and the switching circuit were covered by the piece of the absorber to minimize its effect on the radiation patterns. Some inconsistency is observed between the measured and simulated results, which is justifiable

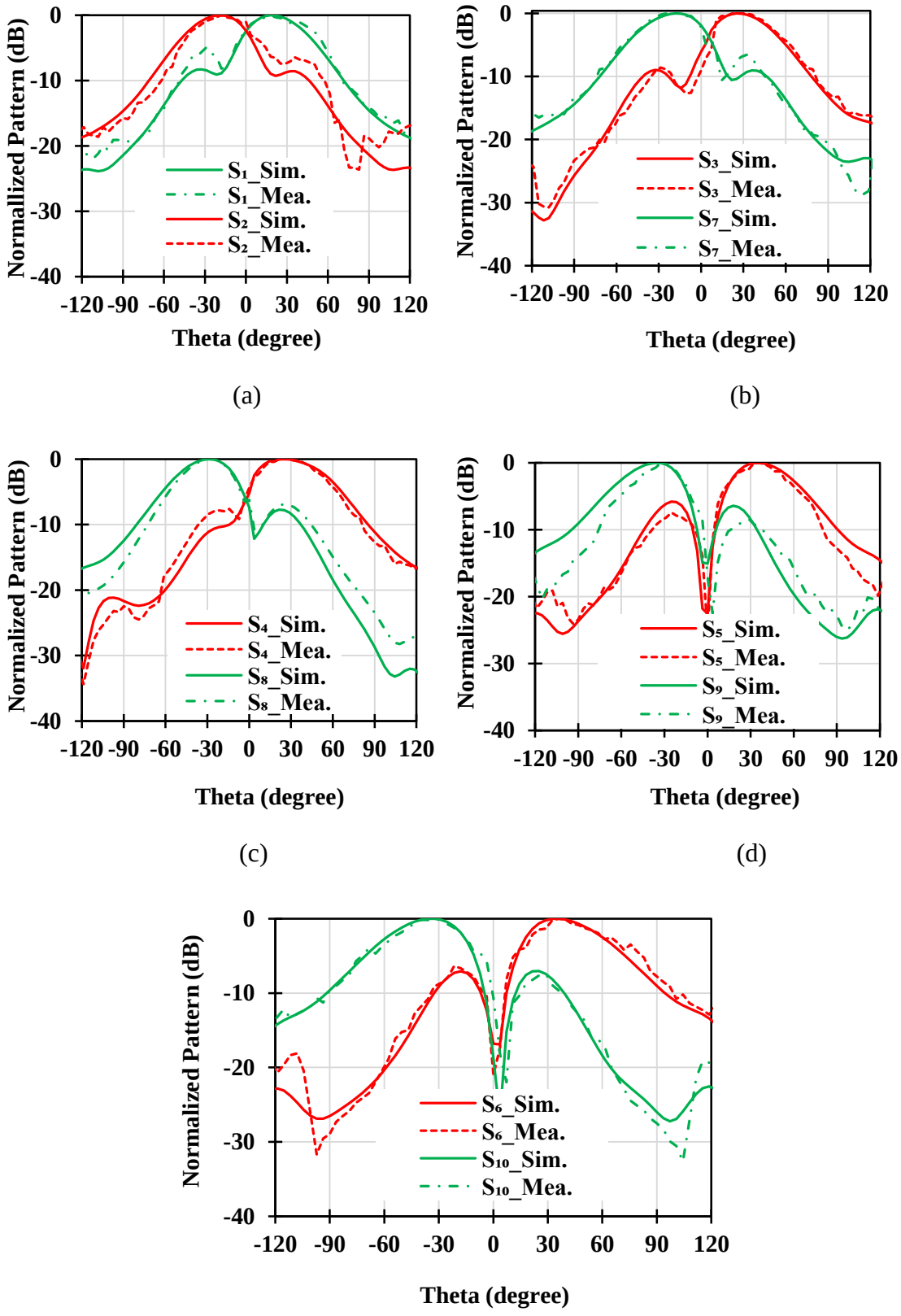

Figure 3.12: The proposed array antenna measured and simulated normalized radiation pattern at the XZ cut plane (a) LHCP, RHCP (b) LHCP (c) RHCP (d) LHCP (e) RHCP.

because the measured results are affected by several parameters, such as approximated modeling of the PIN diode from the datasheet that does not represent the exact behavior of the PIN diode in real, the effect of the external switching circuit, DC voltage source and the reflections from the biasing line.

The measured results demonstrate that the proposed beam steerable and circular polarization reconfigurable antenna can simultaneously reconfigure the polarization between the LHCP and RHCP and steer its radiation beam between -30° to +30° for both polarization states.

3.4 Comparison and Review

A comparison between the existing works with similar function or structure and proposed antenna is listed in Table 3.4. The polarization reconfigurable antenna presented in [63], and [76] are low profile but they can only be reconfigurable in one property which further limits its application. Antenna reported in [133] has the wide impedance bandwidth and 3 dB ARBW but the problem of reconfigurability in single property still remains the same.

In [83] and [143] both pattern and polarization can be reconfigured using 2x2 patch array antenna but their beam switching range and 3 dB axial ratio bandwidth are smaller than the proposed work. Beam switching range in [144] and [145] are larger than the proposed antenna and also axial ratio bandwidth in [145] are comparable to the proposed antenna but at the same time they require more array elements as compared to this work. Furthermore, the proposed antenna has the smallest dimension compared to [83], [143], [144] and [145].

Therefore, the proposed reconfigurable antenna can perform beam switching and polarization reconfiguration characteristics using a compact structure and minimum number of antenna elements. Besides, the proposed antenna has the advantages of wide impedance bandwidth, wide 3 dB axial ratio bandwidth for two CP modes, and wide

steering angle for the pattern reconfiguration mode.

Table 3.4: **Comparison of the proposed array antenna characteristics with previously reported work**

Ref.	NAE	D (λ_0)^3	CF (GHz)	PRM	BSR (°)	IMBW (%)	ARBW (%)	NS
[63]	1	0.65x1.14x0.08	2.45	LHCP/RHCP	NA	7	8.8	2
[76]	1	0.57x0.57x0.06	2.45	LHCP/RHCP/LP	NA	13.1	9.4	8
[133]	1	0.61x0.61x0.26	2.45	LHCP/RHCP/LP	NA	33	30	8
[83]	2x2	1.6x1.6x0.07	4.8	LHCP/RHCP	-16 to +16	9	4.2	28
[143]	2x2	1.33x1.33x0.07	5.4	LHCP/RHCP	-22 to +22	16.8	6	40
[144]	1x4	0.85x2.34x0.05	2.53	LHCP/RHCP	-40 to +40	14.7	8	60
[145]	1x4	1.87x2.34x0.33	2.25	LHCP/RHCP/LP	-40 to +40	38.5	18	24
This Work	1x2	1.04x1.04x0.19	5.2	LHCP/RHCP	-30 to +30	23	17.4	20

Here λ_0 = free space wavelength at the center frequency, NAE = no. of antenna elements, D = dimensions, CF = center frequency, PRM = polarization reconfigurable modes, BSR = beam scanning range, IMBW = impedance bandwidth ARBW = axial ratio bandwidth, NS = no. of Switches,

3.5 Summary

A beam steerable and circular polarization reconfigurable antenna consisting of an E-shaped patch antenna element, a phase switchable transmission line based power divider, and four switchable feeding probes has been developed. In the proposed antenna, four feed probes are connected to the patch through four PIN diodes. By switching the states of four PIN diodes, polarization of the antenna has been reconfigured among two CP states, i.e., LHCP and RHCP. The prototype of the proposed concept has been fabricated and tested. A reasonable agreement between the simulated and measured results has been achieved. Upto ± 30° beam-switching for both LHCP and RHCP states has been realized using this

array antenna. The proposed active antenna design with circular polarization agility and beam switching capability holds potential for a wide range of applications in the 4 to 7 GHz frequency band, including low-band 5G communication systems such as 5G n79 band, wireless communication, radar, satellite, and medical and scientific systems.

After successful implementation of the circular polarization reconfigurable beam steering antenna, a quad-polarization reconfigurable stacked array antenna with 2-D beam switching is proposed in the next chapter.